Environmental Science and Pollution Research (2019) 26:25476–25490
https://doi.org/10.1007/s11356-019-05852-1

RESEARCH ARTICLE

Synthesis of functionalized mesoporous material from rice husk ash and its application in the removal of the polycyclic aromatic hydrocarbons

José Arnaldo S. Costa[1,2] · Victor H. V. Sarmento[3] · Luciane P. C. Romão[4] · Caio M. Paranhos[2]

Received: 18 April 2019 / Accepted: 24 June 2019 / Published online: 1 July 2019

Abstract

The rice husk ash (RHA) was used as an alternative source of silica for the synthesis of the functionalized mesoporous material, which was used in the removal of the PAHs naphthalene (Nap), benzo[b]fluoranthene (B[b]F), benzo[k]fluoranthene (B[k]F), and benzo[a]pyrene (B[a]P) from aqueous media. The PABA-MCM-41 (RHA) was characterized using FTIR, TGA, SAXS, and N_2 adsorption–desorption analyses. Removal experiments were performed to determine the initial concentrations, individual adsorption in comparison with the mixture of the PAHs, PABA-MCM-41 (RHA) amount, pH, time, and temperature, and the results obtained were statistically analyzed. The PABA-MCM-41 (RHA) presented the S_{BET}, V_T, and D_{BJH} values of 438 $m^2\ g^{-1}$, 0.41 $cm^3\ g^{-1}$, and 3.59 nm, respectively, and good thermal stability. The q_e values found in the kinetic equilibrium for the PAHs mixture followed increasing order: Nap < B[a] P < B[k]F < B[b]F, with removal percentages of 89.08 ± 0.00, 93.85 ± 0.28, 94.54 ± 0.10, and 97.80 ± 0.05%, respectively.

Keywords Rice husk ash · Functionalized mesoporous material · PABA-MCM-41 (RHA) · Adsorption · PAHs

Introduction

Organic compounds have attracted a lot of attention from environmental monitoring programs, mainly because of their toxic, persistent, and resist degradation effects (Busso et al. 2018). Among the groups of persistent organic compounds, it is possible to indicate the polycyclic aromatic hydrocarbons (PAHs) (Dat and Chang 2017). Due to the properties of PAHs, they are monitored in the environment by the United States Environmental Protection Agency (U.S. EPA 1993), while that the International Agency for Research on Cancer (IARC) classifies that some of these PAHs are carcinogenic to humans (Conama 2005; IARC 2010; Brasil 2011; Costa et al. 2017a; Dat and Chang 2017; Busso et al. 2018; Sigmund et al. 2018; Wołejko et al. 2018).

Thus, waste recycling can be an attractive alternative to reduce the impacts that are caused to the environment from the incorrect destination of industrial waste (Costa and Paranhos 2018). Rice is one of the foods most consumed by the Brazilian population, so Brazil is one of the main world producers of this cereal (FAO 2017). World rice production as well as the number of planted areas has been increasing since 2009, where world rice production was over 724 million tons and the area planted was over 158 million ha (FAO 2017). However, Brazilian rice production between the years 2013–2017 is around 11 million tons, and the South Region is the largest producer of the grain (FAO 2017).

The rice husk (RH) represents approximately 20 wt% of the paddy produced (Costa and Paranhos 2018). Particles in suspension from RHs burned or buried can cause serious respiratory diseases to humans as well as impacts on the

Responsible editor: Tito Roberto Cadaval Jr

Electronic supplementary material The online version of this article (https://doi.org/10.1007/s11356-019-05852-1) contains supplementary material, which is available to authorized users.

✉ José Arnaldo S. Costa
josearnaldo@ua.pt

[1] CICECO, Department of Chemistry, University of Aveiro, 3810-193 Aveiro, Portugal

[2] Polymer Laboratory, Department of Chemistry, Federal University of São Carlos, São Carlos, São Paulo 13565-905, Brazil

[3] Department of Chemistry, Federal University of Sergipe, Itabaiana, Sergipe 49100-000, Brazil

[4] Department of Chemistry, Federal University of Sergipe, São Cristóvão, Sergipe 49100-000, Brazil

environment (An et al. 2010). The use of dispersed sources of energy, in particular biomass, appears as an important opportunity, mainly in the conversion of biomass to energy (Foletto et al. 2005; Costa and Paranhos 2018). The rice husk ash (RHA) can contain about 99% by mass of silica (Panpa and Jinawath 2009) and can be used as an inexpensive alternative source of amorphous silica to produce silicon-based nanostructured materials of technological interest. The use of an alternative source of silica is an important factor not only in the textural and structural properties of mesostructured material obtained, but also at the economic cost to synthesize this material. It is known that the synthesis of silicon-based nanostructured materials from a commercial silica source, such as tetraethyl orthosilicate (TEOS) or tetramethyl orthosilicate (TMOS), is relatively expensive. In addition, recycling of industrial waste, such as RH, can be an attractive alternative to reduce impacts on the environment and human health, thereby allowing the sustainable development of new advanced multifunctional materials.

Among these materials, it is possible to highlight the mesoporous molecular sieves of the M41S family. The mesoporous material has an ordered mesoporous structure, with a hexagonal arrangement of uniformly sized and well-defined pores. Some intrinsic characteristics, such as high surface area, constant mesopore size distribution, and stability in the adsorption process, are common to this material. Consequently, the reuse of mesoporous materials after adsorption process can be easily achieved (Santos et al. 2013; Costa et al. 2014, 2015, 2017a). Wastewater pollution can be mitigated by adsorption process based in the mesoporous material (Lee et al. 2007; Wang et al. 2012). In this study, PABA-MCM-41 (RHA) mesoporous material synthesized from rice husk ash was used for the adsorption of the PAHs from aqueous media.

Experimental

Standards, solvents, and reagents

The rice husk was provided from the Brazilian Agricultural Research Corporation (Embrapa), São Carlos, São Paulo, Brazil. Thermal treatment performed to obtain RHA from RH and characterizations of the RH and RHA are reported previously (Costa and Paranhos 2018, 2019). The Nap, B[b]F, B[k]F, and B[a]P analytical standards (> 96.0% purity) were obtained from Aldrich. The solvent utilized was HPLC-grade acetonitrile (99.9%, Tedia). Cetyltrimethylammonium bromide (CTAB, 98.0%, NEON), p-aminobenzoic acid (PABA, ≥ 99.0%, Aldrich), 3-(triethoxysilyl)propyl isocyanate (TEPIC, Aldrich), and ammonia monohydrate ($NH_3 \cdot H_2O$, Synth) were all used without further purification. Ultrapure water was obtained from a Milli-Q system (Millipore Co.).

Synthesis of the PABA-MCM-41 (RHA) mesoporous material

The modification of the PABA was performed according to the methodology described previously (Costa et al. 2014), and the hydrothermal/co-condensation synthesis of the PABA-MCM-41 (RHA) followed the methodology described previously (Costa et al. 2014) and the procedure described by Appaturi et al. (2012), with modifications. Details of the synthesis procedure are suitable in Supplementary Information.

Characterizations of the mesoporous material

The FTIR spectra and thermogravimetric analysis (TGA) analyses were obtained according to the methodology described previously (Costa et al. 2017a). Small-angle X-ray scattering (SAXS) experiments were performed according to the methodology described previously (Costa et al. 2015). SEM image was performed in a Phillips FEG-XL 30 microscopy, using an accelerator power of 3 kV and analyzed with the help of a secondary electron detector. Nitrogen adsorption–desorption isotherms were measured according to the methodology described previously (Costa et al. 2015). However, the sample was evacuated at 150 °C for 1 h in the degas port of the instrument.

Batch experiments

The removal experiments were conducted for evaluation of the initial PAH (Nap, B[a]P, B[b]F, and B[k]F) concentrations; individual adsorption in comparison with the mixture of the PAHs, PABA-MCM-41 (RHA) amount, pH, time, and temperature were conducted in amber flasks at 25 °C, with orbital agitation speed of 150 rpm. All the adsorption experiments were performed in duplicate, as previously reported (Costa et al. 2017a). The PAH concentrations were determined using an HPLC instrument (Shimadzu, Japan) equipped with a fluorescence detector. The adsorbed PAH amount was calculated using Eq. (1):

$$q_e = \frac{(C_0 - C_e)V}{m}. \quad (1)$$

where C_o and C_e are the before and after concentrations of the PAHs (μg L^{-1}) in the adsorption process, respectively, q_e is the amount of the PAHs adsorbed (μg g^{-1}), m is the mass of the PABA-MCM-41 (RHA) (g), and V is the volume of the solution (L).

Change in the initial PAH concentration

The same conditions related in item 2.4 was employed to investigate the initial PAH solution concentration. The overall

time was adjusted to 24 h for the concentration range of 50–1700 μg L^{-1}.

Change in the individual adsorption in comparison with the mixture of the PAHs

Test was performed to investigate the adsorption capacity of PAHs in individual solution and in a mixture containing the four PAHs, for an exposure time of 24 h.

Change in the solution pH

The removal of a mixture of Nap, B[a]P, B[b]F, and B[k]F by PABA-MCM-41 (RHA) was studied at pH 3, 5, 9, 11, and non-adjusted pH (pH_{in}) to determine the optimum solution pH, with a time of 24 h. The initial concentration of the mixture was 200 μg L^{-1}.

Change in the PABA-MCM-41 (RHA) amount

The adsorbent amount was investigated in the range 10–100 mg of PABA-MCM-41 (RHA), exposure time of 24 h, concentration of 200 μg L^{-1} of the PAHs, and solution pH equal at initial (5.6).

Change in the contact time

Different exposure times in the range 0–600 min were investigated using a concentration of 200 μg L^{-1}, initial solution pH, and 50 mg of each sample.

Change in the temperature

Removal of the PAHs as a function of temperature by the samples was evaluated using temperatures of 25, 40, and 55 °C, exposure times between 0 and 600 min, concentration of 200 μg L^{-1}, initial solution pH, and 50 mg of the PABA-MCM-41 (RHA).

Regeneration of the PABA-MCM-41 (RHA)

To further investigate the performance of the mesoporous material, reuse experiments were carried out. At the end of the adsorption, the saturated adsorbent was separated by filtration, washing, and drying at 70 °C for 24 h. The regenerated adsorbent was reused in the next runs under the same conditions.

Statistical analysis

ANOVA was used for the q_e means of the repetitions of tests, and the results were compared via the Tukey test at 5% probability, using version 8.0 of the Origin software.

Kinetic study and adsorption isotherms

Two kinetics models, pseudo-first- and pseudo-second-order, were used to investigate the adsorption equilibrium data. Isothermal measurements were performed at 25, 40, and 55 °C. The obtained data were fitted using the Langmuir and Freundlich isotherm models.

Determination of the PAHs

Quantification of the PAHs was done using a Shimadzu HPLC LC-20A Prominence instrument according to the methodology described previously (Costa et al. 2017a). The values of the linear correlation coefficients (r^2) obtained to the calibration curves were 0.996, 0.997, 0.999, and 0.999 for Nap, B[a]P, B[b]F, and B[k]F, respectively.

Results and discussion

Characterization of the mesoporous materials

FTIR

The FTIR spectra obtained for the pure and modified PABA, as well as PABA-MCM-41 (RHA) mesoporous material, are shown in Fig. 1a–c. In the spectrum of the pure PABA (Fig. 1a), it is possible to observe the main characteristic bands of the PABA. The bands centered at 3459, 3363, and 3231 cm^{-1} are assigned to the N–H bond of the amino groups (NH_2). The band at around 1670 cm^{-1} and those at around 1442 and 1422 cm^{-1} are assigned to C=O and C=C bonds of the carboxylic acid and aromatic ring of the PABA, respectively. However, the bands located at around 1174 and 1128 cm^{-1} are attributed to the C–N bond of the Ar–NH_2 groups (Pavia et al. 2001). The FTIR spectrum for the modified PABA (PABA-Si) (Fig. 1b) exhibited absorption bands that confirms the presence of the TEPIC into PABA, as well as the PABA-MCM-41 (RHA) (Fig. 1c) presented the same characteristic bands of the functionalized mesoporous material, as demonstrated previously (Costa et al. 2014) in the synthesis of PABA-MCM-41 from the use of tetraethylorthosilicate (TEOS) as the source of silica.

SAXS

The SAXS profile for the PABA-MCM-41 (RHA) is shown in Fig. 1d. From the analysis of Fig. 1d, it is possible to observe that the ratio of the relative distances between the peaks ($q_{1\,0\,0}$/$q_{1\,0\,0}$, $q_{1\,1\,0}$/$q_{1\,0\,0}$, and $q_{2\,0\,0}$/$q_{1\,0\,0}$), which were 1:√3:2, respectively, confirms the mesostructure of the PABA-MCM-41 (RHA), as demonstrated previously (Costa et al. 2014, 2019), confirming the successful synthesis of the

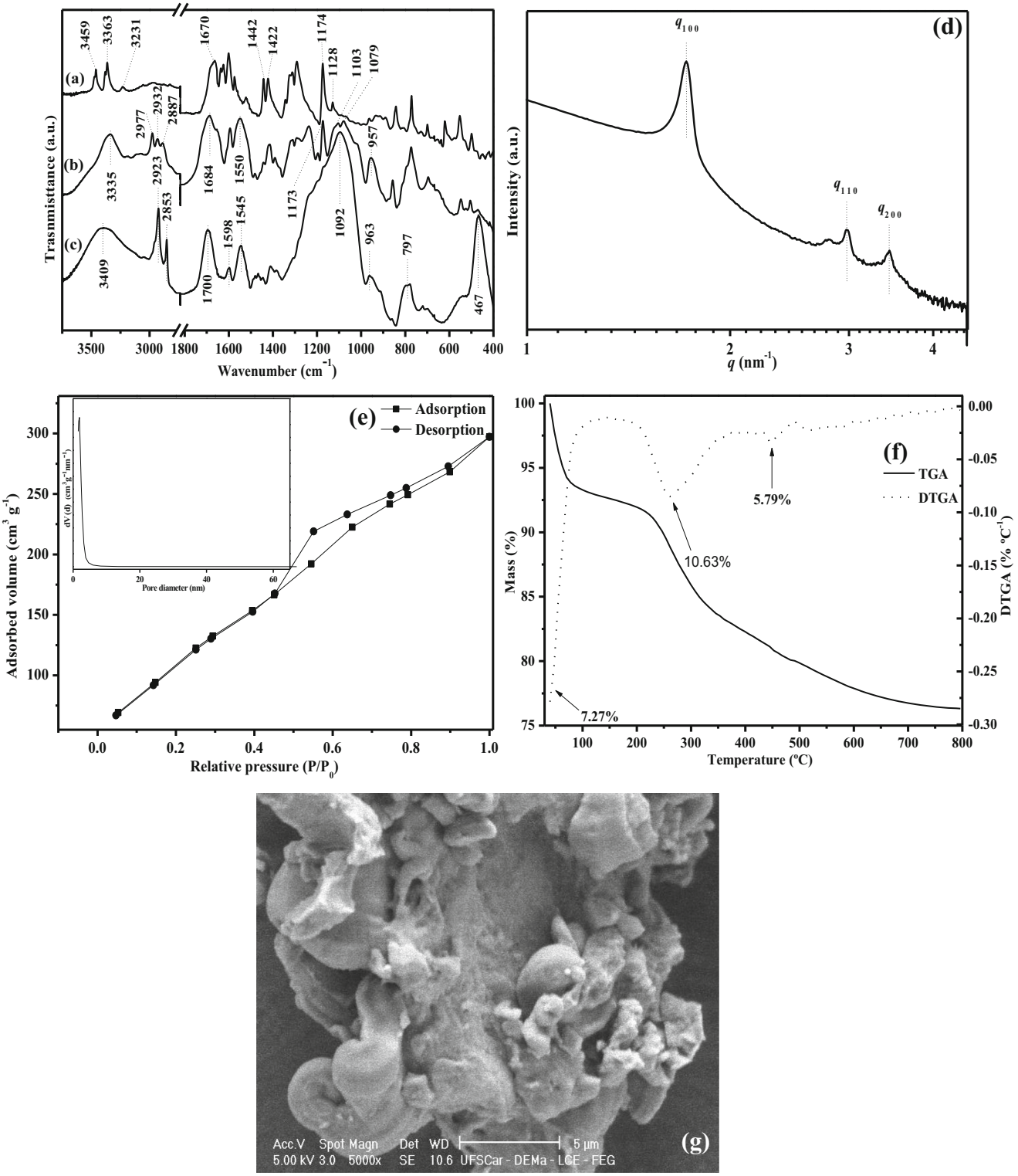

Fig. 1 FTIR spectra of (a) PABA, (b) PABA-Si, and (c) PABA-MCM-41 (RHA), X-ray scattering intensity (d), nitrogen adsorption/desorption isotherms (e), TGA/DTGA curves (f), and SEM image for the PABA-MCM-41 (RHA) mesoporous material

PABA-MCM-41 (RHA) from the use of the silica from RHA as an alternative and inexpensive source of amorphous silica. The calculated d and a_0 values for the PABA-MCM-41 (RHA) are presented in Table 1.

Nitrogen adsorption–desorption isotherms

Figure 1 e shows the nitrogen adsorption–desorption isotherms for the PABA-MCM-41 (RHA), as well as the pore

Table 1 Textural and structural properties of the PABA-MCM-41 (RHA) mesoporous material

Mesoporous material	$d_{1\,0\,0}$ (nm)	S_{BET} ($m^2\ g^{-1}$)	V ($cm^3\ g^{-1}$)	V_T ($cm^3\ g^{-1}$)	D_{BJH} (nm)	a_0 (nm)	W_T (nm)
PABA-MCM-41 (RHA)	3.64	438	0.28	0.41	3.59	4.20	0.61
PABA-MCM-41 (RHA)-HPAs	–	157	0.05	0.11	1.69	–	–

$d_{1\,0\,0}$ $d(1\,0\,0)$ spacing, a_0 center–center distance ($a_0 = (2/\sqrt{3})d$), S_{BET} BET surface area, V pore volume, V_T total pore volume, D_{BJH} pore diameter, W_T wall thickness, calculated as $a_0 - D_{BJH}$

size distribution (Fig. 1e inset). It is possible to observe that the PABA-MCM-41 (RHA) presented type IV isotherms with H1 hysteresis (Costa et al. 2014, 2015, 2017a; Santos et al. 2019).

The S_{BET} and D_{BJH} calculated values are summarized in Table 1. The decrease in the S_{BET}, V, V_T, and D_{BJH} values for the PABA-MCM-41 (RHA)-PAHs after adsorption process was attributed to the adsorption of the PAHs into the pores of the mesoporous material.

TGA

Figure 1 f shows the TGA/DTGA curves obtained for the PABA-MCM-41 (RHA). It is possible to observe that the PABA-MCM-41 (RHA) showed mass loss event in the ranges 35–139 °C; this event can be attributed to the loss of H_2O and residual solvents physically adsorbed in the PABA-MCM-41 (RHA). The second event (at 177–391 °C) was attributed to decomposition of the organic matter (OM) of the modified p-aminobenzoic acid (PABA-Si) in the functionalized mesoporous material. Finally, the third event, in the range 414–750 °C, was associated to combustion of the residual OM of the PABA-Si groups situated within the pores of the PABA-MCM-41 (RHA) (Costa et al. 2014, 2015).

SEM

Figure 1 g shows the SEM image obtained for the PABA-MCM-41 (RHA) functionalized mesoporous material. The SEM image was used to determine the morphology of the synthesized mesoparticles, and the PABA-MCM-41 (RHA) presented a surface with the agglomerated quasi-spherical particles (Costa et al. 2014, 2015, 2017b).

Batch adsorption experiments and statistical analysis

Change in the initial PAHs concentration: Individual adsorption in comparison with the mixture of the PAHs

Figure 2 a illustrates the evaluation of the initial concentration of the PAH individual solution in the adsorption by PABA-MCM-41 (RHA). As shown in Fig. 2a, the amount of the PAHs adsorbed increased when the initial concentrations were higher. In this way, we can observe that q_e values found for B[b]F, B[k]F, and B[a]P were higher than the values found for adsorption of Nap by mesoporous material. This same comportment was reported by Costa et al. (2012) and Liu et al. (2011). They related that the adsorbed amount by an adsorbent material increases with increasing molecular mass and the number of aromatic rings of the PAHs. For a direct comparison, the Nap has a molecular mass of 128 g mol^{-1} and 2 aromatic rings. In contrast, B[b]F, B[k]F, and B[a]P are structural isomers of molecular mass equal to 252 g mol^{-1} and 5 aromatic rings. Thus, the similarity of the results for B[b]F, B[k]F, and B[a]P can be attributed to the similar chemical characteristics of these compounds (Costa et al. 2017a).

The evaluation of the initial concentration in the adsorption of the mixture of the PAHs by PABA-MCM-41 (RHA) is shown in Fig. 2b. The q_e values also increased with increasing of concentration of the mixture of the PAHs. Similarly, the structural isomerism of B[b]F, B[k]F, and B[a]P also influenced in adsorption of the PAHs mixture by PABA-MCM-41 (RHA). However, the q_e values found for the PABA-MCM-41 (RHA) from the concentration of 800 μg L^{-1} in the adsorption of B[b]F, B[k]F, and B[a]P followed the decreasing order of q_e values: B[b]F > B[a]P > B[k]F.

In general, it is possible to observe that the q_e values found in the adsorption of B[b]F, B[k]F, and B[a]P by mesoporous material increase linearly with increasing individual concentration of these PAHs. However, for the tests with the PAHs mixture, the q_e values tend to reach equilibrium at the higher concentrations. This can be due to the increase in the number of the PAH molecules competing by active sites of the PABA-MCM-41 (RHA), as well as the saturation of these active sites. However, the efficiency or maximum adsorption capacity of the PAHs will be better evaluated from the comparison of these experimental results with the Freundlich and Langmuir adsorption isotherm models. Finally, it is important to mention that even the q_e values being slightly higher for the individual solution tests, the other adsorption tests were performed using the PAHs mixture PAHs, because a solution of the PAHs mixture can best represent a real sample of wastewater.

The results obtained in the adsorption process were submitted to an ANOVA, as shown in Tables 2 and 3 for the individual and mixture adsorption of the PAHs, respectively, and it can be seen that there are significant differences in the mean q_e

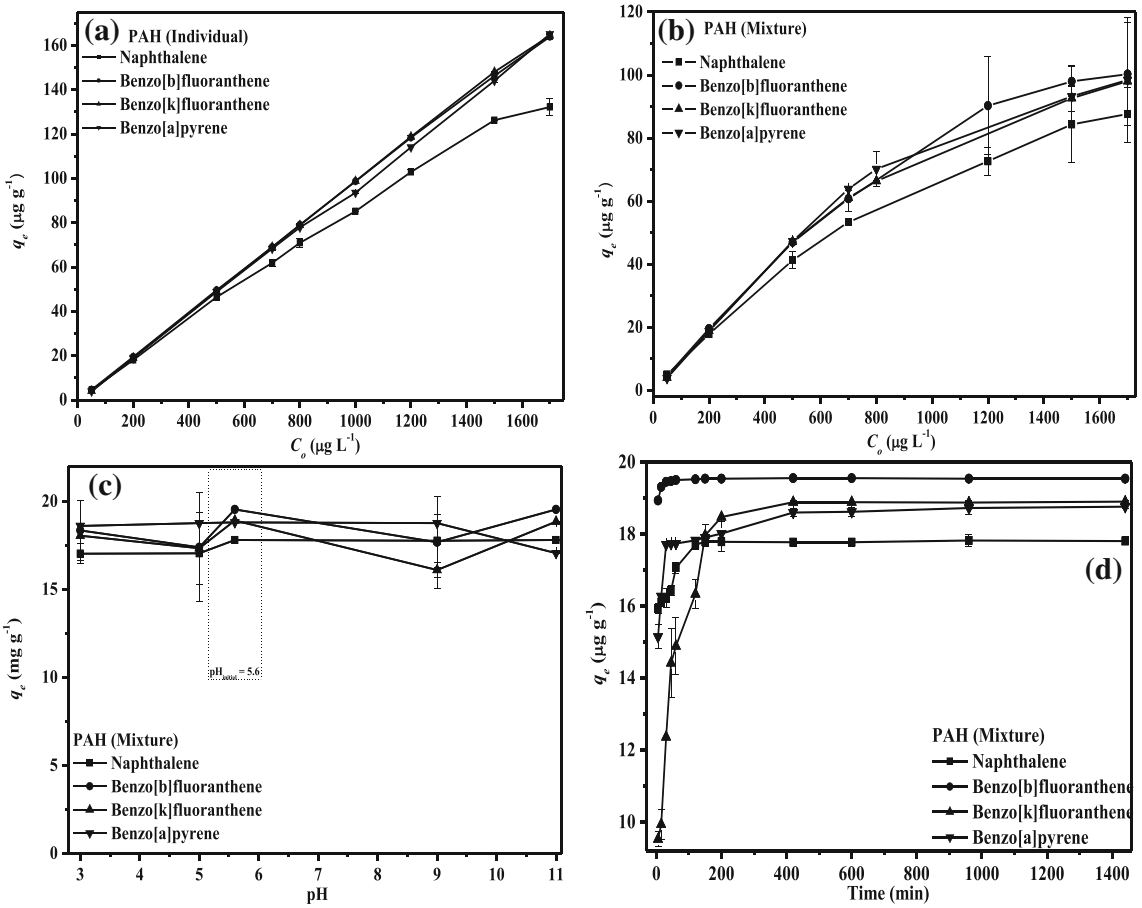

Fig. 2 Change of initial concentration in adsorption (**a**) individual and (**b**) mixture of the PAHs, solution pH (**c**), and contact time (**d**) by PABA-MCM-41 (RHA) mesoporous material

for both processes at the 5% significance level, the F-tabulated values are equal to 3.23 and 3.87, respectively, for 8 and 9 degrees of freedom (*DF*) in the individual and 6 and 7 in the mixture adsorption. Thus, as the F-calculated values were higher than the F-tabulated values, it can be said that at least two of the means are not equal at the 5% significance level. Thus, in order to establish the minimum significant difference between the means of the different adsorption processes, the Tukey test had to be applied in order to identify which means are statistically different at 5% probability.

Figure S1 shows the results of the Tukey test for the means q_e for individual adsorption of the PAHs. It can be seen that all means present statistical differences for the adsorption of B[b]F, B[k]F, and B[a]P; however, the same was not observed for the concentrations of 1500 and 1700 μg L^{-1} for Naf, which have no statistical differences. The results of the Tukey test for the means q_e for mixture adsorption of the PAHs are shown Fig. S2, it can be seen that the concentrations of 50–200, 500–700, 700–1200, 1200–1500, 1200–1700, and 1500–1700 μg L^{-1} for Naf, 50–200, 200–500, 500–700, 700–1200, 1200–1500, 1200–1700, and 1500–1700 μg L^{-1} for B[b]F, 700–800, and 1500–1700 μg L^{-1} for B[k]F, 50–200, 200–500, 500–700, 500–800, 700–800, 700–1500, 800–1500, 800–1700, and 1500–1700 μg L^{-1} for B[a]P have no statistical differences.

Change of solution pH

The pH change can alter the surface of the PABA-MCM-41 (RHA), as well as the degree of ionization of the adsorbate in aqueous medium. However, the chemical properties of the PAHs, which are compounds considered inert, therefore do not have ionizable groups that can be altered by the medium pH (Zeledón-Toruño et al. 2007; Hu et al. 2014). However, a variation in the solution pH may significantly alter the surface charges of the adsorbent mesoporous material.

Figure 2 c shows the pH change in the adsorption of the PAH mixture by PABA-MCM-41 (RHA). It is possible to observe that pH change between 3 and 11 does not significantly affect the adsorption capacity of the PABA-MCM-41 (RHA) by Nap, B[b]F, and B[k]F, as well as between 5 and 9 in the adsorption of B[a]P. However, there was a small decrease in the q_e values for Nap in the pH values of 3 and 5, for B[b]F and B[k]F at pH 3, 5, and 9, and at pH 11 for B[a]P.

Same not affecting in the ionization of the PAHs, the pH variation can affect the surface charges of the PABA-MCM-

Table 2 Analysis of variance parameters for the variation of initial concentration in adsorption individual of the PAHs by PABA-MCM-41 (RHA) mesoporous material

Source of variation	*DF*	*SS*	*MS*	*F*
Naf				
Treatments	8	31,833.69	3979.21	1419.95[a]
Residual	9	25.22	2.80	
Total	17	31,858.91		
B[b]F				
Treatments	8	47,077.44	5884.68	26,938.95[a]
Residual	9	1.97	0.22	
Total	17	47,079.41		
B[k]F				
Treatments	8	48,151.58	6018.95	1.29×10^{10}[a]
Residual	9	4.21×10^{-6}	4.67×10^{-7}	
Total	17	48,151.58		
B[a]P				
Treatments	8	46,453.01	5806.63	48,313.71[a]
Residual	9	1.08	0.12	
Total	17	46,454.09		

DF degrees of freedom, *SS* sum of squares, *MS* mean squared, *F* F-statistic value

[a] Significant at the 5% probability level ($0.01 \leq p < 0.05$)

41 (RHA), at pH < 7. There is a considerable amount of H^+ ions, and these ions are responsible for the protonation of the

Table 3 Analysis of variance parameters for the variation of initial concentration in adsorption mixture of the PAHs by PABA-MCM-41 (RHA) mesoporous material

Source of variation	DF	SS	MS	*F*
Naf				
Treatments	6	12,470.52	2078.42	85.69[a]
Residual	7	169.78	24.25	
Total	13	12,640.30		
B[b]F				
Treatments	6	17,710.46	2951.74	37.77[a]
Residual	7	547.05	78.15	
Total	13	18,257.51		
B[k]F				
Treatments	6	14,794.28	2465.71	819.85[a]
Residual	7	21.05	3.01	
Total	13	14,815.33		
B[a]P				
Treatments	6	15,259.07	2543.18	34.37[a]
Residual	7	518.00	74.00	
Total	13	15,777.07		

DF degrees of freedom, *SS* sum of squares, *MS* mean squared, *F* F-statistic value

[a] Significant at the 5% probability level ($0.01 \leq p < 0.05$)

carboxylic acid groups ($-CO_2H$) of the PABA-Si in the PABA-MCM-41 (RHA) (Putra et al. 2009).

$$-CO_2H + H^+ \rightarrow -CO_2H_2^+ \quad (2)$$

Thus, positive charges in the PABA-MCM-41 (RHA) cause an increase in the electrostatic interaction between the surface of the PABA-MCM-41 (RHA) with the π electrons of the PAHs (Balati et al. 2015; Lamichhane et al. 2016). However, at very low pH, there is an excess of H^+ ions, and these ions can compete with the PAH molecules in the adsorption process in the active sites, resulting in a decrease in adsorbed amount, as can be observed for Nap, B[b]F, and B[k]F at pH 3 and 5.

On the other hand, at pH > 7, a large amount of OH^- ions exists, which now promote deprotonation of the $-CO_2H$ groups (Putra et al. 2009):

$$-CO_2H + OH^- \rightarrow -CO_2^- \quad (3)$$

Thus, these OH^- ions compete and/or interact with the PAH molecules in the adsorption on the active sites of the PABA-MCM-41 (RHA), and this reflects in the reduction of the capacity of the adsorption (Balati et al. 2015; Lamichhane et al. 2016). Therefore, this behavior was observed in the pH 9 in the adsorption of B[b]F and B[k]F, and at pH 11 for B[a]P; however, this was not observed for Nap. Based on the results obtained of the pH effect, the initial pH value (5.6) was chosen to be used in the other tests.

ANOVA parameters obtained for the adsorption of Naf, B[b]F, and B[k]F from pH change show that there are no significant differences in the mean q_e for these processes, as shown in Table S1e and Figs. S3a–c. However, in the pH change for adsorption of B[a]P, it is possible to observe that there is difference between the means of the results of q_e; as can be seen in Table S1, the T-calculated value is much greater than the F-tabulated value (5.19).

Figure S3 shows the mean difference from the Tukey test for pH change in the adsorption of the PAHs. From the analysis of Fig. S3d, it is possible to observe that only the pH 5–5.6, 5–9, and 5.6–9 do not present statistical difference in the adsorption of B[a]P.

Change of PABA-MCM-41 (RHA) dosage

The influence of the adsorbent amount in the adsorption of the PAHs mixture by PABA-MCM-41 (RHA) is shown in Fig. S4. The results indicated that the adsorbent amount increases with the increase of the PABA-MCM-41 (RHA) mass. However, the increase of the q_e values for the PAHs B[b]F and B[a]P was practically insignificant, and this small increase can be attributed to the increased surface area and the availability of more adsorption sites (Santos et al. 2013). Based on the results obtained, the adsorption dosage of 50 mg was used

for the further studies to evaluate the effect of other parameters.

Thus, from the ANOVA parameters obtained for the adsorption of Naf, B[b]F, and B[a]P, it is possible to observe that the change of PABA-MCM-41 (RHA) dosage is not significantly different in the q_e values, as shown in Table S2e and Figs. S5a, b, and d, since the T-calculated value is less than that the F-tabulated value (6.59). However, only dosages of 5 and 100 mg have statistical difference for the adsorption of B[k]F, according to the results of Table S2 and Fig. S5c.

Change of contact time

Figure 2 d shows the evaluation of exposure time in the adsorption of the PAH mixture by PABA-MCM-41 (RHA). There was an increase of the q_e value with the time, with fast adsorption in the first 60 min (for Nap and B[b]F) and a slower process in equilibrium. The adsorption equilibrium was reached after approximately 150 and 200 min for B[k]F e B[a]P, respectively.

The q_e values found in the kinetic equilibrium in the adsorption of the PAHs mixture Nap, B[b]F, B[k]F, and B[a]P by PABA-MCM-41 (RHA) were 17.83 ± 0.16, 19.56 ± 0.01, 18.91 ± 0.02, and 18.77 ± 0.06 μg g^{-1}, respectively, with the adsorption increasing in the order: Nap < B[a]P < B[k]F < B[b]F. At equilibrium, their respective percentage removal values were 89.08 ± 0.00, 93.85 ± 0.28, 94.54 ± 0.10, and 97.80 ± 0.05%.

In general, the q_e value found for Nap was lower than the values found for the other PAHs. However, for the PAH

Table 4 Comparation of adsorption efficiency of the PAHs mixture by PABA-MCM-41 (RHA) functionalized mesoporous material with other absorbent materials reported in the literature

Material	Compound	Adsorption capacity	Efficiency (%)	Reference
Si-MCM-41	Benzo[k]fluoranthene	18.26 μg g^{-1}	90.40	(Costa et al. 2017a)
	Benzo[b]fluoranthene	18.35 μg g^{-1}	90.84	
	Benzo[a]pyrene	18.78 μg g^{-1}	92.98	
PABA-MCM-41	Benzo[a]pyrene	27.20 μg g^{-1}	96.20	(Costa et al. 2014)
MCM-41	Benzo[k]fluoranthene	12.49 μg g^{-1}	–	(Costa et al. 2015)
	Benzo[b]fluoranthene	18.06 μg g^{-1}		
PABA-MCM-41	Benzo[k]fluoranthene	22.51 μg g^{-1}	–	(Costa et al. 2015)
	Benzo[b]fluoranthene	26.58 μg g^{-1}		
MCM-41	Naphthalene	0.69 mmol g^{-1}	–	(Araújo et al. 2008)
BOW	Benzo[k]fluoranthene	15.66 μg g^{-1}	66.92	(Jesus et al. 2019)
	Benzo[a]pyrene	17.25 μg g^{-1}	68.78	
BEG	Benzo[k]fluoranthene	17.25 μg g^{-1}	73.75	(Jesus et al. 2019)
	Benzo[a]pyrene	18.88 μg g^{-1}	75.29	
BGW	Benzo[k]fluoranthene	10.88 μg g^{-1}	54.69	(Jesus et al. 2019)
	Benzo[a]pyrene	17.11 μg g^{-1}	77.28	
BCW	Benzo[k]fluoranthene	18.09 μg g^{-1}	78.51	(Jesus et al. 2019)
	Benzo[a]pyrene	21.01 μg g^{-1}	81.94	
Activated sludge	Naphthalene	–	28.90	(Liu et al. 2011)
Periodic mesoporous organosilica	Naphthalene	–	70.00	(Vidal et al. 2011)
Activated carbon	Benzo[k]fluoranthene	–	80.00	(Gong et al. 2007)
	Benzo[b]fluoranthene		84.00	
	Benzo[a]pyrene		85.00	
Immature coal (leonardite)	Benzo[a]pyrene	–	82.00	(Zeledón-Toruño et al. 2007)
	Benzo[k]fluoranthene		82.00	
HZSM-5	Naphthalene	–	75.60	(Costa et al. 2012)
HUSY			71.60	
HZSM-5	Benzo[k]fluoranthene	–	47.60	(Costa et al. 2012)
HUSY			43.90	
HZSM-5	Benzo[b]fluoranthene	–	62.90	(Costa et al. 2012)
HUSY			69.50	
PABA-MCM-41 (RHA)	Naphthalene	17.83 μg g^{-1}	89.08	This study
	Benzo[b]fluoranthene	19.56 μg g^{-1}	97.80	
	Benzo[k]fluoranthene	18.91 μg g^{-1}	94.54	
	Benzo[a]pyrene	18.77 μg g^{-1}	93.85	

isomers (B[b]F, B[k]F, and B[a]P), this adsorption process could also be explained by the effect of hydrophobicity of the PAHs in solution. The hydrophobic molecules were surrounded by water, and these molecules forming a cage that promoted stronger hydrophobic interactions, thus stabilizing the less soluble PAH molecules in the solution (Costa et al. 2017a). Hence, the PAH molecules that were more soluble in water were able to interact more easily with the carboxylic acid groups of the PABA-MCM-41 (RHA).

Also, if we correlate the above ideas with the values of the octanol-water partition coefficient (K_{ow}), which is correlated with the degree of lipophilic affinity of a compound, it is possible to predict that the higher the log K_{ow} value, more hydrophobic will be the compound (less soluble). Therefore, as the log K_{ow} values for B[a]P, B[k]F, and B[b]F are 6.04, 6.00, and 5.80, respectively (De Maagd et al. 1998; Nam et al. 2001; Latimer and Zheng 2003; Ribeiro and Ferreira 2003), it is now possible to interconnect these log K_{ow} values with the sequence of q_e values obtained. In the literature, some studies show the adsorption efficiency of different adsorbent material; for example, Liu et al. (2011) obtained a percentage removal of Nap of 28.90% using inorganic particles and activated sludge, and Vidal et al. (2011) found a removal efficiency of 70.00% using periodic mesoporous organosilica. Gong et al. (2007) used activated carbon for removal of the PAHs and achieved average removals of B[k]F, B[b]F, and B[a]P of 80.0, 84.0, and 85.0%, respectively. Zeledón-Toruño et al. (2007) obtained a B[a]P and B[k]F removal efficiency of 82.0%, using an immature coal (leonardite). Costa et al. (2012) reported removal values of 75.60 and 71.60% for Nap, 47.60 and 43.90% for B[k]F, 62.90 and 69.50% for B[b]F, and 43.80 and 37.20% for B[a]P, using the zeolite materials HZSM-5 and HUSY as adsorbents, respectively.

In our previous work, we found 96.20% of individual removal of B[a]P using the functionalized mesoporous material PABA-MCM-41 (Costa et al. 2014), and q_e values of 12.49 and 18.06 μg g^{-1} for B[k]F, and 22.51 and 26.58 μg g^{-1} in the individual removal of the PAHs with the MCM-41 and PABA-MCM-41 mesoporous materials, respectively (Costa et al. 2015). The removal of B[k]F, B[b]F, and B[a]P mixture by Si-MCM-41 obtained a removal efficiency of 90.40, 90.48, and 92.98%, respectively (Costa et al. 2017a). Therefore, Table 4 shows the comparation of adsorption efficiency of the PAHs mixture by PABA-MCM-41 (RHA) functionalized mesoporous material with other absorbent materials reported in the literature (Gong et al. 2007; Zeledón-Toruño et al. 2007; Araújo et al. 2008; Liu et al. 2011; Vidal et al. 2011; Costa

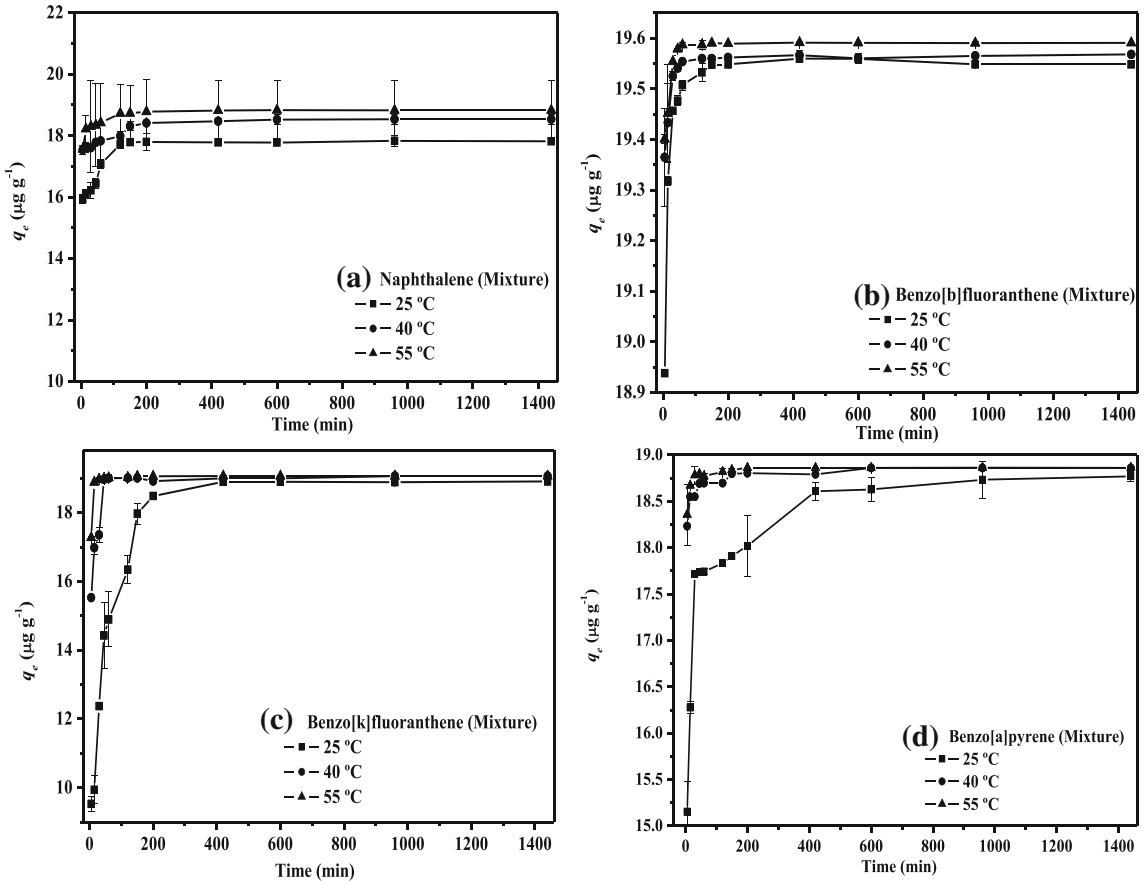

Fig. 3 Change of temperature in adsorption of the PAHs mixture by PABA-MCM-41 (RHA) mesoporous material

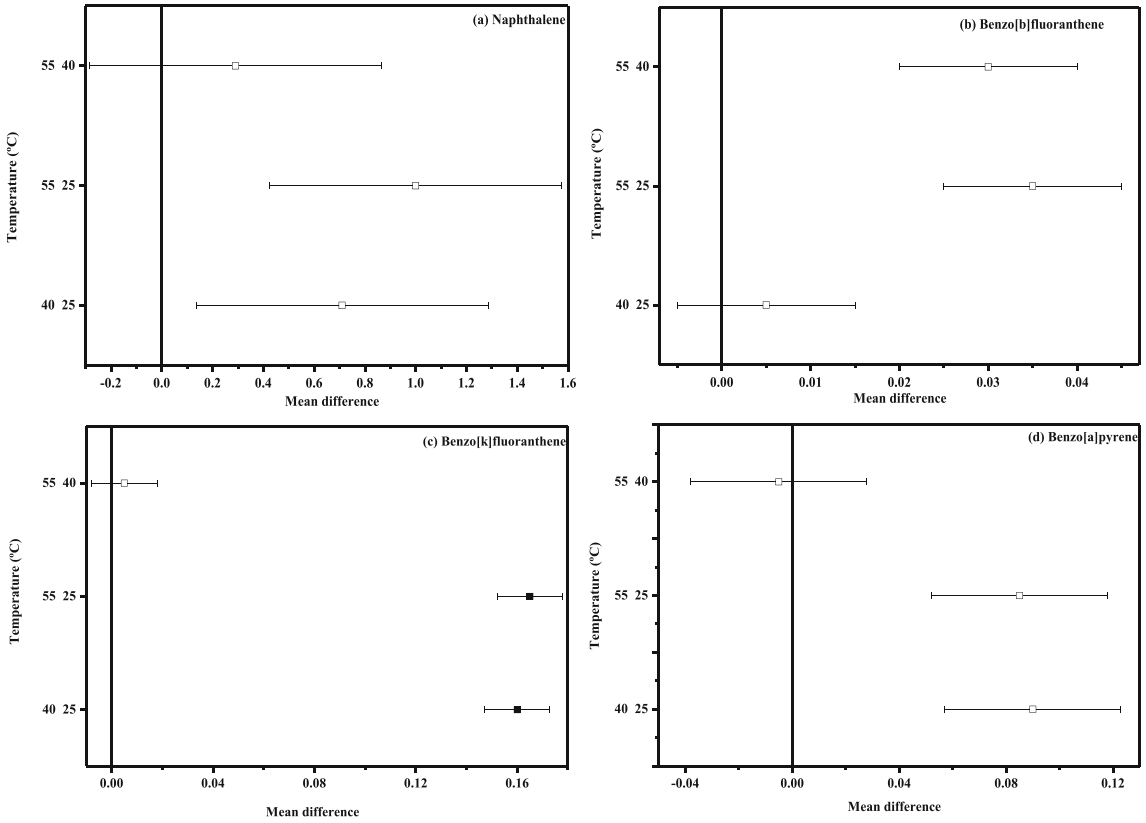

Fig. 4 Means comparison from Tukey test for the change of temperature in adsorption of the PAH mixture by PABA-MCM-41 (RHA) mesoporous material

et al. 2012, 2014, 2015, 2017a; Jesus et al. 2019). It can be concluded that PABA-MCM-41 (RHA) provided excellent removal efficiency of the PAH mixture; therefore, the results indicate that PABA-MCM-41 (RHA) can be used as adsorbent material for the removal of different organic compounds from surface water or wastewater.

Table 5 Comparison of the pseudo-first- and pseudo-second-order kinetic models on the adsorption of the PAHs mixture by PABA-MCM-41 (RHA) mesoporous material

PAH	T (°C)	$q_{e\ (exp.)}$ (μg g^{-1})	Pseudo-first order				Pseudo-second order			
			$q_{e\ (cal.)}$ (μg g^{-1})	k_1 (min^{-1})	h_i ((μg g^{-1})^2 min^{-1})	r^2	$q_{e\ (cal.)}$ (μg g^{-1})	k_2 (g μg^{-1} min^{-1})	h_i (μg g^{-1} min^{-1})	r^2
PABA-MCM-41 (RHA)										
Nap	25	17.83 ± 0.16	17.31 ± 0.21	0.50 ± 0.11	151.05 ± 51.76	0.183	17.53 ± 0.18	0.08 ± 0.03	23.20 ± 13.75	0.604
	40	18.53 ± 0.16	18.14 ± 0.15	0.68 ± 0.14	224.68 ± 70.39	0.096	18.24 ± 0.11	0.20 ± 0.07	65.68 ± 34.04	0.440
	55	18.83 ± 0.97	18.62 ± 0.07	0.57 ± 0.05	198.63 ± 26.62	0.595	18.73 ± 0.05	0.15 ± 0.02	51.55 ± 10.32	0.861
B[b]F	25	19.56 ± 0.01	19.51 ± 0.02	0.71 ± 0.03	268.70 ± 16.93	0.838	19.56 ± 0.00	0.31 ± 0.01	117.80 ± 5.41	0.996
	40	19.57 ± 0.00	19.55 ± 0.01	0.94 ± 0.05	358.06 ± 27.55	0.626	19.56 ± 0.01	0.92 ± 0.09	350.41 ± 49.21	0.906
	55	19.59 ± 0.00	19.57 ± 0.01	0.95 ± 0.05	362.75 ± 27.61	0.569	19.59 ± 0.01	0.94 ± 0.11	361.60 ± 60.22	0.862
B[k]F	25	18.91 ± 0.02	17.88 ± 0.79	0.05 ± 0.01	16.18 ± 6.53	0.626	18.72 ± 0.60	0.01 ± 0.00	1.78 ± 0.32	0.845
	40	19.06 ± 0.00	18.69 ± 0.22	0.35 ± 0.05	120.83 ± 9.01	0.603	19.04 ± 0.14	0.04 ± 0.01	15.00 ± 5.43	0.876
	55	19.06 ± 0.00	19.02 ± 0.02	0.48 ± 0.01	172.37 ± 5.63	0.989	19.15 ± 0.05	0.11 ± 0.01	38.85 ± 5.48	0.926
B[a]P	25	18.77 ± 0.06	18.02 ± 0.21	0.36 ± 0.05	116.37 ± 26.82	0.574	18.35 ± 0.13	0.05 ± 0.01	15.22 ± 5.10	0.867
	40	18.86 ± 0.00	18.74 ± 0.03	0.72 ± 0.05	253.23 ± 25.98	0.607	18.79 ± 0.02	0.32 ± 0.04	113.04 ± 20.31	0.859
	55	18.86 ± 0.01	18.82 ± 0.02	0.74 ± 0.03	262.77 ± 15.81	0.829	18.86 ± 0.01	0.38 ± 0.01	136.76 ± 5.23	0.986

Table 6 Activation energies and Arrhenius frequency factors calculated for the adsorption of PAHs mixture by PABA-MCM-41 (RHA) mesoporous material

Mesoporous material	PAH	E_a (kJ mol^{-1})	A (g μg^{-1} min^{-1})	r^2
PABA-MCM-41 (RHA)	NaP	15.81 ± –	5.35×10^{1} ± –	–
	B[b]F	30.75 ± 15.76	8.83×10^{4} ± 431.29	0.584
	B[k]F	82.81 ± 15.80	1.92×10^{12} ± 439.18	0.930
	B[a]P	58.77 ± 26.14	1.17×10^{9} ± 23.48×10^{3}	0.700

E_a activation energy, A Arrhenius frequency factor

Change of temperature

The change of temperature was performed to obtain the rate constants, and the calculation of the activation energy (E_a) was performed using the Arrhenius equation according to the methodology described previously (Costa et al. 2014, 2015).

The change of temperature in adsorption process of the PAHs mixture by PABA-MCM-41 (RHA) is shown in Fig. 3. As can be seen in Fig. 3, there was an increase of the initial rate of adsorption with the increase of the temperature from 25 to 55 °C, and it is possible to observe an increase of the q_e value with the elevation of temperature in the adsorption of Nap. However, the same was not observed for the other PAHs.

However, the ANOVA analysis (Table S3) showed that only the results obtained from the change of temperature in the adsorption of B[k]F show statistical differences, since the T-calculated value is greater than that the F-tabulated value (9.55), and the Tukey test showed that the temperature of 25 °C is different from the others, according to the results of Fig. 4.

Kinetics of adsorption

The first- and second-order kinetic models have been used according to the methodology described in our previous works (Costa et al. 2015, 2017a). Table 5 shows the comparison of the first- and second-order kinetic models in the adsorption of the PAHs mixture by PABA-MCM-41 (RHA). The best fit of the experimental data was obtained with the pseudo-second-order model, as shown by the r^2 values, compared to those found using the pseudo-first-order model.

The r^2 values found for the pseudo-second-order model ranged from 0.440 to 0.996 in the adsorption process, and the $q_{e(exp.)}$ values were very close to the $q_{e(cal.)}$ values calculated from the pseudo-second-order model. As discussed above, where it was possible to observe that the temperature variation between 25 and 55 °C did not cause such a significant variation of the q_e values, however, this increase affected the initial rate of adsorption of process. It is possible to observe the increase of the k_2 and h_i values for the pseudo-second-order model (except for Nap at 55 °C), and the k_2 and h_i values found in the adsorption of the PAH mixture can be ordered in increasing order as follows: B[k]F < Nap < B[a]P < B[b]F.

The E_a and A values in the adsorption process by PABA-MCM-41 (RHA) are summarized in Table 6. The magnitude of the E_a value can indicate whether the adsorption process occurs by a mechanism of physisorption or chemisorption; some studies found in the literature suggest that processes governed by physisorption present E_a values between 5 and 40 kJ mol^{-1} and between 40 and 800 kJ mol^{-1} for

Table 7 Comparison of equilibrium data obtained using the Freundlich and Langmuir isotherm models applied to the adsorption of the PAHs by PABA-MCM-41 (RHA) mesoporous material

		Freundlich			Langmuir		
Mesoporous material	PAH	K_F (L g^{-1})	n	r^2_F	Q_{max} (μg g^{-1})	b (L μg^{-1})	r^2_L
PABA-MCM-41 (RHA)	Individual						
	Nap	6.15 ± 1.90	1.88 ± 0.21	0.952	190.77 ± 17.65	0.007 ± 0.001	0.976
	B[b]F	20.96 ± 6.83	1.91 ± 0.35	0.822	229.20 ± 35.71	0.047 ± 0.016	0.898
	B[k]F	18.52 ± 11.28	1.78 ± 0.60	0.449	270.86 ± 120.97	0.033 ± 0.025	0.510
	B[a]P	7.61 ± 6.93	1.45 ± 0.49	0.641	256.49 ± 145.98	0.017 ± 0.016	0.677
	Mixture						
	Nap	7.64 ± 1.37	2.72 ± 0.22	0.987	98.19 ± 4.67	0.008 ± 0.001	0.985
	B[b]F	13.40 ± 3.78	3.14 ± 0.46	0.939	104.49 ± 5.66	0.022 ± 0.006	0.968
	B[k]F	11.85 ± 4.43	3.05 ± 0.60	0.871	101.79 ± 7.45	0.018 ± 0.005	0.945
	B[a]P	14.00 ± 5.97	3.29 ± 0.80	0.795	104.02 ± 7.81	0.022 ± 0.006	0.936

Table 8 Values of the dimensionless separation factor (R_L) obtained from the equilibrium data on the adsorption of the PAHs by PABA-MCM-41 (RHA) mesoporous material

Mesoporous material	PAH	Individual R_L	Mixture
PABA-MCM-41 (RHA)	Nap	0.42 ± 0.05	0.38 ± 0.04
	B[b]F	0.10 ± 0.05	0.19 ± 0.06
	B[k]F	0.13 ± 0.22	0.22 ± 0.07
	B[a]P	0.23 ± 0.50	0.19 ± 0.06

chemisorption processes (Özcan and Özcan 2004; Almeida et al. 2009; Cottet et al. 2014). It is possible to observe that the E_a values found in adsorption of Nap and B[b]F by PABA-MCM-41 (RHA) are among the adsorption range of a mechanism proposed by a physisorption, and are an indication that adsorption has a low potential barrier. However, for the values of B[a]P and B[k]F, it is possible to observe that these are in the range of values between a chemisorption process, but these values are very close to the limit of the physisorption, so we suggest that these processes also occur by this same adsorption mechanism. In addition, if we consider the physical-chemical properties of the PAHs, which are non-ionizable molecules, we can expect that there is an electrostatic interaction between the surface of the adsorbent with the π electrons of the PAHs.

Based on the theory that the higher the E_a value, the slower the adsorptive process, so the greater the energy barrier of adsorption. Therefore, it is possible to observe that the E_a value was higher for B[k]F, followed by B[a]P, B[b]F, and Nap. Finally, the results obtained for the E_a values were low, compared to the higher values that are found in chemisorption processes (40–800 kJ mol^{-1}); thus, low E_a values indicate that the initial adsorption velocity is little influenced by the elevation of temperature, which in fact was confirmed by the k_2 and h_i values found at the temperatures studied.

The A value is related to the impacts between the PAH molecules and the PABA-MCM-41 (RHA) (Costa et al. 2014, 2015). The A values increased with the increase of the E_a values, and this is due to the fact that the higher the E_a value of an adsorptive process, the lower the initial adsorption velocity. Therefore, this process will require more effective

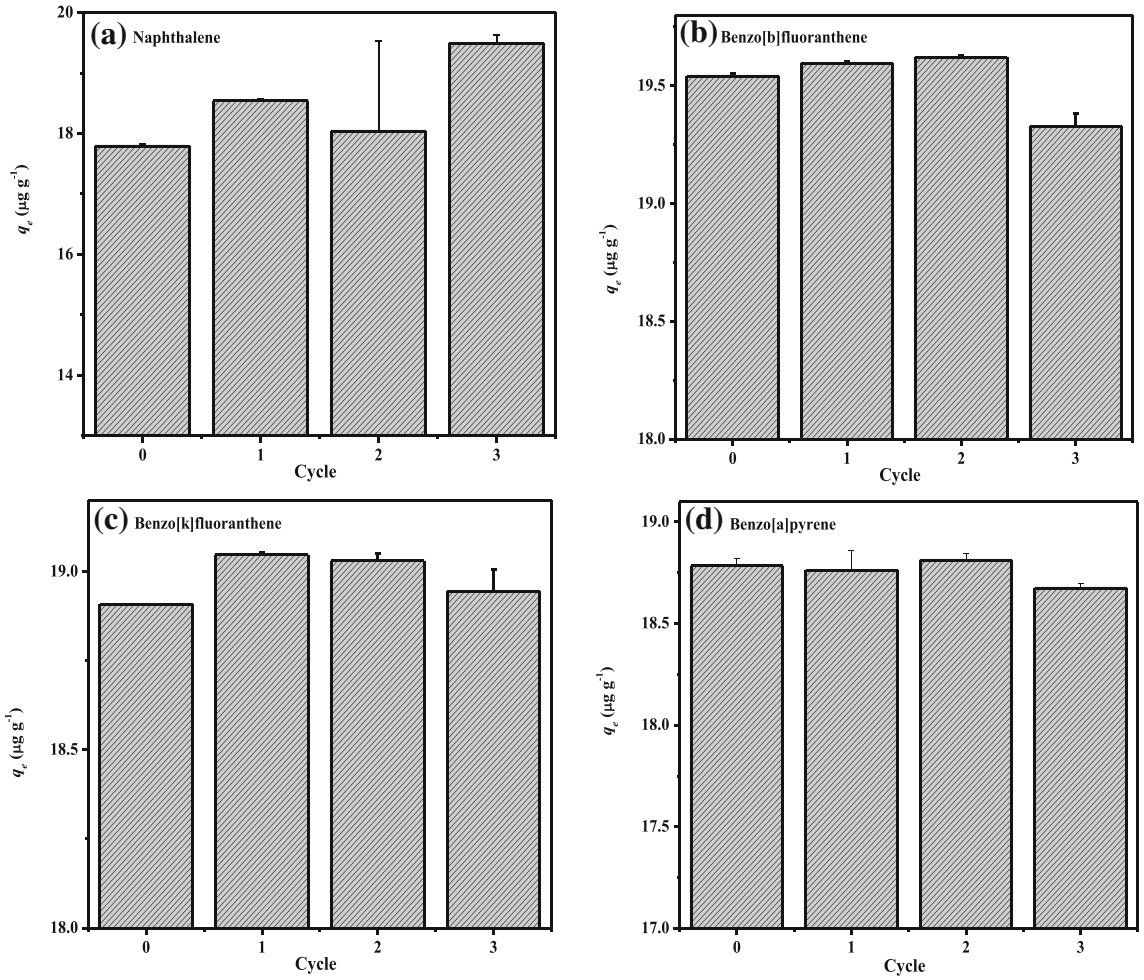

Fig. 5 Reuse cycles of PABA-MCM-41 (RHA) mesoporous material in the adsorption of the PAH mixture (**a**) Nap, (**b**) B[b]F, (**c**) B[k]F, and (**d**) B[a]P

impacts between the PAH molecules with the active sites of the PABA-MCM-41 (RHA) in order to achieve the adsorption equilibrium.

Adsorption isotherms

Adsorption data have been used according to the methodology described in our previous works (Costa et al. 2015, 2017a). Moreover, the isotherm model is a way of predicting whether the adsorption is favorable or unfavorable, and this is done by calculating a dimensionless separation factor (*RL*) given by the following equation (Wang et al. 2017):

$$R_L = \frac{1}{1 + bC_o} \tag{4}$$

where C_o is the initial PAH concentration (μg L^{-1}) and b (L μg^{-1}) is the Langmuir constant. Thus, the adsorption process is considered unfavorable if the value of $R_L > 1$, linear for $R_L = 1$, irreversible for $R_L = 0$, and favorable for $0 < R_L < 1$.

Table 7 shows the equilibrium data obtained in the adsorption of the PAHs by PABA-MCM-41 (RHA). So, the experimental data were more closely fitted using the Langmuir model, for which the r^2 values were higher. The Langmuir model is more suitable than Freundlich to describe the adsorption process (Costa et al. 2014). In the adsorption of the individual PAHs by PABA-MCM-41 (RHA), it is possible to observe that the Q_{max} value was higher in the adsorption of B[k]F compared to other PAHs, and the Q_{max} values found can be ordered in descending order as follows: B[k]F > B[a]P > B[b]F > Nap.

In the adsorption of the PAH mixture by PABA-MCM-41 (RHA), it is possible to observe that the Q_{max} values obtained in the adsorption of B[b]F, B[k]F, and B[a]P were very close to each other. However, the Q_{max} values found in the adsorption of the HPAs individual were higher than the values obtained from the adsorption of the mixture of the same. This is due to the simultaneous adsorption of the PAHs, as well as a competition between these PAHs by the adsorption sites of the adsorbent material.

Table 8 shows the results of the R_L values found from the adsorption of the PAHs by PABA-MCM-41 (RHA). Therefore, it is possible to observe that the R_L values are between the range $0 < R_L < 1$, confirming that the adsorption process of these PAHs (individual and mixture) by mesoporous material occurs by a favorable mechanism.

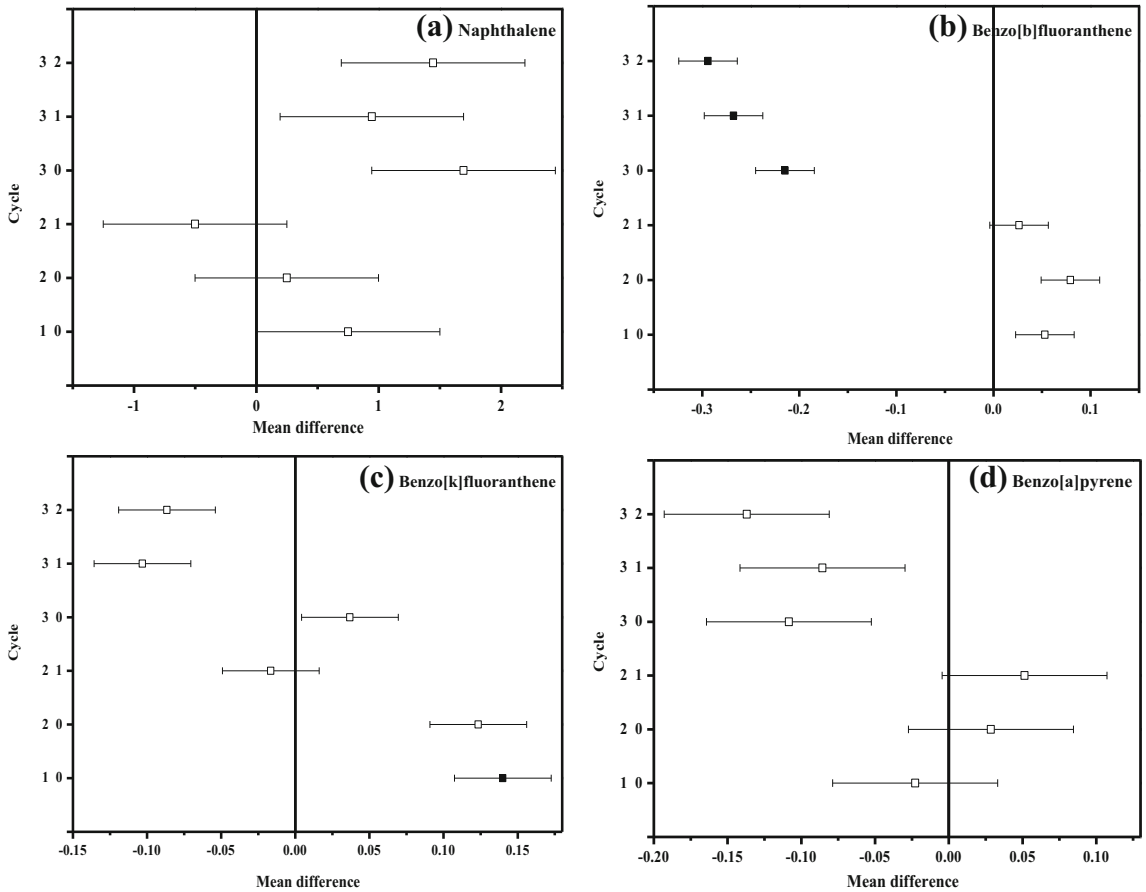

Fig. 6 Means comparison from Tukey test for the reuse cycles of PABA-MCM-41 (RHA) mesoporous material in the adsorption of the PAHs mixture (**a**) Nap, (**b**) B[b]F, (**c**) B[k]F, and (**d**) B[a]P

Regeneration of the adsorbent

The reuse of an adsorbent material is a very important characteristic, once these can be regenerated and reused in the other adsorption processes. Figure 5 shows the results obtained from the reuse cycles of PABA-MCM-41 (RHA) in the adsorption of the PAH mixture. In the adsorption of Nap (Fig. 5a), the adsorption efficiency increased in the 1st and 3rd adsorption cycles. In the adsorption of B[b]F and B[a]P (Fig. 5b, d), it is possible to observe a slight decrease in the adsorption efficiency in the 3rd cycle. In contrast, in the adsorption of B[b]F (Fig. 5c), it is possible to observe that the adsorption efficiency in the 1st, 2nd, and 3rd adsorption cycles was higher than the value found for the initial material. In general, it is possible to affirm that the PABA-MCM-41 (RHA) mesoporous material tested did not present significant losses of adsorption efficiency from their reuses, which are good results for an application of these materials in systems of remediation of xenobiotic pollutants such as PAHs.

The results obtained in the different cycles of the adsorption were submitted to an ANOVA. According to Table S4, it is possible to observe that there are statistical differences for the results obtained for B[b]F and B[k]F, since the T-calculated values are greater than that the F-tabulated value (6.59). Thus, it is possible to observe that only the 3rd cycle is different from the others, in adsorption of B[b]F (Fig. 6b), and there is only difference between the initial and 1st cycle in the adsorption of B[k]F (Fig. 6).

Conclusions

The PABA-MCM-41 (RHA) mesoporous material presented bands characteristic of the amorphous condensed silica framework, hexagonal mesostructure, and high surface area. The synthesis of PABA-MCM-41 (RHA) from the amorphous silica extracted of the RHA as alternative source of silica was confirmed from the characterization techniques used.

The adsorption tests of the PAHs by PABA-MCM-41 (RHA) showed that there was an increase in the q_e values with the increase of the initial concentration, amount of the adsorbent, and contact time; however, the temperature variation was not very significant, and the best pH value was the initial. The adsorption equilibrium was relatively rapid and followed the nonlinear pseudo-second-order and Langmuir theoretical models.

The q_e values found in the kinetic equilibrium for the PAHs mixture (Nap, B[b]F, B[k]F, and B[a]P) followed the increasing order: Nap < B[a]P < B[k]F < B[b]F, with removal percentages of 89.08 ± 0.00, 93.85 ± 0.28, 94.54 ± 0.10, and 97.80 ± 0.05%, respectively.

Funding information This work was supported by FAPESP (Research Support Foundation of the State of São Paulo) (Grants 2014/05679-4, 2017/06775-5, and 2018/18894-1), CAPES (Coordination for the Improvement of Higher Education Personnel) (Grant 309342/2010-4), and CDMF (Center for the Development of Functional Materials) (Grant 2013/07296-2) for the financial support and LNLS for the SAXS measurements (Project SAXS1 12642).

Compliance with ethical standards

Conflict of interest The authors declare that they have no conflict of interest.

References

Almeida CAP, Debacher NA, Downs AJ et al (2009) Removal of methylene blue from colored effluents by adsorption on montmorillonite clay. J Colloid Interface Sci 332:46–53. https://doi.org/10.1016/j.jcis.2008.12.012

An D, Guo Y, Zhu Y, Wang Z (2010) A green route to preparation of silica powders with rice husk ash and waste gas. Chem Eng J 162:509–514. https://doi.org/10.1016/j.cej.2010.05.052

Appaturi JN, Adam F, Khanam Z (2012) A comparative study of the regioselective ring opening of styrene oxide with aniline over several types of mesoporous silica materials. Microporous Mesoporous Mater 156:16–21. https://doi.org/10.1016/j.micromeso.2012.01.023

Araújo RS, Azevedo DCS, Cavalcante CL et al (2008) Adsorption of polycyclic aromatic hydrocarbons (PAHs) from isooctane solutions by mesoporous molecular sieves: influence of the surface acidity. Microporous Mesoporous Mater 108:213–222. https://doi.org/10.1016/j.micromeso.2007.04.005

Balati A, Shahbazi A, Amini MM, Hashemi SH (2015) Adsorption of polycyclic aromatic hydrocarbons from wastewater by using silica-based organic–inorganic nanohybrid material. J Water Reuse Desalin 5:50. https://doi.org/10.2166/wrd.2014.013

Brasil (2011) Ministério da Saúde. Portaria MS Nº 2914 12 Dezembro 2011 2011:32

Busso IT, Tames F, Silva JA et al (2018) Biomonitoring levels and trends of PAHs and synthetic musks associated with land use in urban environments. Sci Total Environ 618:93–100. https://doi.org/10.1016/j.scitotenv.2017.10.295

Conama (2005) Resolução n 357, 18 de março de 2005. Diário Of 58–63

Costa JAS, Paranhos CM (2018) Systematic evaluation of amorphous silica production from rice husk ashes. J Clean Prod 192:688–697. https://doi.org/10.1016/j.jclepro.2018.05.028

Costa JAS, Paranhos CM (2019) Evaluation of rice husk ash in adsorption of Remazol Red dye from aqueous media. SN Appl Sci 1:1–8. https://doi.org/10.1007/s42452-019-0436-1

Costa AA, Wilson WB, Wang H et al (2012) Comparison of BEA, USY and ZSM-5 for the quantitative extraction of polycyclic aromatic hydrocarbons from water samples. Microporous Mesoporous Mater 149:186–192. https://doi.org/10.1016/j.micromeso.2011.06.016

Costa JAS, Garcia ACFS, Santos DO et al (2014) A new functionalized MCM-41 mesoporous material for use in environmental applications. J Braz Chem Soc 25:197–207. https://doi.org/10.5935/0103-5053.20130284

Costa JAS, Garcia ACFS, Santos DO et al (2015) Applications of inorganic-organic mesoporous materials constructed by self-assembly processes for removal of benzo[k]fluoranthene and benzo[b]fluoranthene. J Sol-Gel Sci Technol 75:495–507. https://doi.org/10.1007/s10971-015-3720-6

Costa JAS, de Jesus RA, da Silva CMP, Romão LPC (2017a) Efficient adsorption of a mixture of polycyclic aromatic hydrocarbons (PAHs) by Si–MCM–41 mesoporous molecular sieve. Powder Technol 308: 434–441. https://doi.org/10.1016/j.powtec.2016.12.035

Costa JAS, de Jesus RA, Dorst DD et al (2017b) Photoluminescent properties of the europium and terbium complexes covalently bonded to functionalized mesoporous material PABA-MCM-41. J Lumin 192: 1149–1156. https://doi.org/10.1016/j.jlumin.2017.08.046

Costa JAS, Vedovello P, Paranhos CM (2019) Use of Ionic Liquid as Template for Hydrothermal Synthesis of the MCM-41 Mesoporous Material. Silicon. https://doi.org/10.1007/s12633-019-00121-9

Cottet L, Almeida CAP, Naidek N et al (2014) Adsorption characteristics of montmorillonite clay modified with iron oxide with respect to methylene blue in aqueous media. Appl Clay Sci 95:25–31. https://doi.org/10.1016/j.clay.2014.03.023

Dat ND, Chang MB (2017) Review on characteristics of PAHs in atmosphere, anthropogenic sources and control technologies. Sci Total Environ 609:682–693. https://doi.org/10.1016/j.scitotenv.2017.07.204

De Maagd PG-J, Ten Hulscher DTEM, Van Den Heuvel H et al (1998) Physicochemical properties of polycyclic aromatic hydrocarbons: aqueous solubilities, n-octanol/water partition coefficients, and Henry's law constants. Environ Toxicol Chem 17:251–257. https://doi.org/10.1002/etc.5620170216

U.S. EPA (1993) Provisional guidance forquantitative risk assessment of polycyclic aromatic hydrocarbons. EPA/600/R-:1–28

FAO (2018) Production international trade domestic prices. Rice Market Monitor 21:1–35

Foletto EL, Hoffmann R, Hoffmann RS et al (2005) Applicability of rice husk ash. Quim Nova 28:1055–1060. https://doi.org/10.1590/S0100-40422005000600021

Gong Z, Alef K, Wilke BM, Li P (2007) Activated carbon adsorption of PAHs from vegetable oil used in soil remediation. J Hazard Mater 143:372–378. https://doi.org/10.1016/j.jhazmat.2006.09.037

Hu Y, He Y, Wang X, Wei C (2014) Efficient adsorption of phenanthrene by simply synthesized hydrophobic MCM-41 molecular sieves. Appl Surf Sci 311:825–830. https://doi.org/10.1016/j.apsusc.2014.05.173

IARC (2010) IARC monographs on the evaluation of carcinogenic risks to humans: some non-heterocyclic polycyclic aromatic hydrocarbons and some related exposures. Iarc Monogr Eval Carcinog Risks To Humans 92:1–868

Jesus JF, Matos TT d S, Cunha G d C et al (2019) Adsorption of aromatic compounds by biochar: influence of the type of tropical biomass precursor. Cellulose 26:4291–4299. https://doi.org/10.1007/s10570-019-02394-0

Lamichhane S, Bal Krishna KC, Sarukkalige R (2016) Polycyclic aromatic hydrocarbons (PAHs) removal by sorption: a review. Chemosphere 148:336–353. https://doi.org/10.1016/j.chemosphere.2016.01.036

Latimer JS, Zheng J (2003) The sources, transport, and fate of PAHs in the marine: PART II general characteristics of PAHs. Wiley, Hoboken, pp 8–33

Lee CK, Liu SS, Juang LC et al (2007) Application of MCM-41 for dyes removal from wastewater. J Hazard Mater 147:997–1005. https://doi.org/10.1016/j.jhazmat.2007.01.130

Liu JJ, Wang XC, Fan B (2011) Characteristics of PAHs adsorption on inorganic particles and activated sludge in domestic wastewater treatment. Bioresour Technol 102:5305–5311. https://doi.org/10.1016/j.biortech.2010.12.063

Nam K, Rodriguez W, Kukor JJ (2001) Enhanced degradation of polycyclic aromatic hydrocarbons by biodegradation combined with a modifed Fenton reaction. Chemosphere 45:11–20

Özcan AS, Özcan A (2004) Adsorption of acid dyes from aqueous solutions onto acid-activated bentonite. J Colloid Interface Sci 276:39–46. https://doi.org/10.1016/j.jcis.2004.03.043

Panpa W, Jinawath S (2009) Synthesis of ZSM-5 zeolite and silicalite from rice husk ash. Appl Catal B Environ 90:389–394. https://doi.org/10.1016/j.apcatb.2009.03.029

Pavia DL, Lampman GM, Kriz GS (2001) Introduction to spectroscopy, 3[a]. Thomson Learning, Inc, Washington D. C. 680 p

Putra EK, Pranowo R, Sunarso J et al (2009) Performance of activated carbon and bentonite for adsorption of amoxicillin from wastewater: mechanisms, isotherms and kinetics. Water Res 43:2419–2430. https://doi.org/10.1016/j.watres.2009.02.039

Ribeiro FAL, Ferreira MMC (2003) QSPR models of boiling point, octanol-water partition coefficient and retention time index of polycyclic aromatic hydrocarbons. J Mol Struct THEOCHEM 663:109–126. https://doi.org/10.1016/j.theochem.2003.08.107

Santos DO, Santos MLN, Costa JAS et al (2013) Investigating the potential of functionalized MCM-41 on adsorption of Remazol Red dye. Environ Sci Pollut Res 20:5028–5035. https://doi.org/10.1007/s11356-012-1346-6

Santos LFS, de Jesus RA, Costa JAS et al (2019) Evaluation of MCM-41 and MCM-48 mesoporous materials as sorbents in matrix solid phase dispersion method for the determination of pesticides in soursop fruit (*Annona muricata*). Inorg Chem Commun 101:45–51. https://doi.org/10.1016/j.inoche.2019.01.013

Sigmund G, Poyntner C, Piñar G et al (2018) Influence of compost and biochar on microbial communities and the sorption/degradation of PAHs and NSO-substituted PAHs in contaminated soils. J Hazard Mater 345:107–113. https://doi.org/10.1016/j.jhazmat.2017.11.010

Vidal CB, Barros AL, Moura CP et al (2011) Adsorption of polycyclic aromatic hydrocarbons from aqueous solutions by modified periodic mesoporous organosilica. J Colloid Interface Sci 357:466–473. https://doi.org/10.1016/j.jcis.2011.02.013

Wang L, Han X, Li J et al (2012) Preparation of modified mesoporous MCM-41 silica spheres and its application in pervaporation. Powder Technol 231:63–69. https://doi.org/10.1016/j.powtec.2012.07.044

Wang N, Jin RN, Omer AM, Ouyang XK (2017) Adsorption of Pb(II) from fish sauce using carboxylated cellulose nanocrystal: isotherm, kinetics, and thermodynamic studies. Int J Biol Macromol 102:232–240. https://doi.org/10.1016/j.ijbiomac.2017.03.150

Wołejko E, Wydro U, Jabłońska-Trypuć A et al (2018) The effect of sewage sludge fertilization on the concentration of PAHs in urban soils. Environ Pollut 232:347–357. https://doi.org/10.1016/j.envpol.2017.08.120

Zeledón-Toruño ZC, Lao-Luque C, de las Heras FXC, Sole-Sardans M (2007) Removal of PAHs from water using an immature coal (leonardite). Chemosphere 67:505–512. https://doi.org/10.1016/j.chemosphere.2006.09.047